# Ocean tide loading displacements observed by very long baseline interferometry during IVS-CONT14 campaign

Kamil Teke

[1]Hacettepe University, Department of Geomatics Engineering 06800 Ankara, Turkey
Phone: +90 312 297 6990, E-mail: kteke@hacettepe.edu.tr

**ABSTRACT**

Ocean tide loading (OTL) displacements can be predicted by convolution software, e.g. SPOTL [1], which convolves the elastic load Green's function over the gridded values of global ocean tide models such as FES2014 [2] for the whole oceans. Besides, ocean tide loading (OTL) displacements can be observed with space geodetic techniques. In this study, the amplitudes and Greenwich phase lags for each coordinate component, i.e., radial, west, and south of the principal semi-diurnal ($M_2$, $S_2$, $N_2$, $K_2$) and -diurnal tides ($K_1$, $O_1$, $P_1$, $Q_1$) of OTL displacements were estimated at the very long baseline interferometry (VLBI) sites of the 15 days long continuous VLBI campaign, CONT14, carried out by the International VLBI Service for Geodesy and Astrometry (IVS). In the estimation of the amplitudes and Greenwich phase lags of the tidal constituents, hourly VLBI station coordinate time series were used as observations derived through analyzing 1 hour VLBI sessions of the CONT14 campaign. The estimated amplitudes and Greenwich phase lags of the principal constituents of OTL displacements were compared with the predictions of the state-of-the-art ocean tide models, among others, FES2012 [3,4], FES2014 [2] and TPXO8 [5,6]. Both the amplitudes and the phases between CONT14 estimates and ocean tide models agree to some extent for the $M_2$, $S_2$, $N_2$, $K_1$, and $O_1$ tides at most of the sites and coordinate components. However, for $K_2$, $P_1$, and $Q_1$ tides CONT14 estimates do not converge to those of the model amplitudes and/or phases. Because such a small duration of 15 days long hourly station coordinate time series does not satisfy the minimum period of Rayleigh criterion [7] to distinguish between neighboring frequencies.

**KEYWORDS**: VLBI; CONT14 hourly sessions; ocean tide loading displacements

## 1. INTRODUCTION

Tidal variations of the pressure exerted by the ocean mass to the seafloor, cause harmonic displacements on the crust so-called ocean tide loading (OTL) displacements. Tidal harmonic constituents of the OTL displacements are predicted through convolving several ocean tide models as well as these tides would be resolved from the observations of space geodetic techniques using the so called static and kinematic methods. In the static approach, real (in-phase) and imaginary (out-of-phase) parts of OTL displacement constituents are estimated along with the daily station coordinates as part of daily solutions. Then, the daily estimates of tidal constituents and their covariance information are stacked in a combined solution e.g. using a Kalman Filter e.g., [8-18]. In kinematic approach, station coordinate time series and their formal errors are estimated at sub-daily intervals without reducing the OTL displacements from the observations a priori to the parameter estimation, then the amplitudes and phases of OTL displacement tidal constituents are decorrelated using harmonic analysis e.g., [19-26].

In literature, several OTL displacement estimation studies based on analyzing the observations of VLBI and/or GNSS techniques can be cited. For example, [8] first demonstrated that applying ocean tide model loading corrections to the a priori coordinates of the VLBI stations located near ocean coasts and on islands reduce the post-fit residuals of the VLBI delays (observations) as well as change VLBI station coordinates up to a few centimeters, suggesting the ocean tide loading can be monitored using VLBI. [9] estimated the vertical components of the OTL displacement semidiurnal ($M_2$, $S_2$, $K_2$, $N_2$) and diurnal tidal constituents ($K_1$, $P_1$, $O_1$, $Q_1$) at six VLBI sites from the analysis of daily VLBI sessions carried out every 5th and 7th day of the week since 1984 till late 1992 with linear least-squares when horizontal amplitudes and phases were fixed to those of ocean tide model from [27]. They compared the estimated vertical amplitudes at the corresponding sites to those of the [27] and [28] models. The accuracy of the VLBI observations at that time was not high enough to determine the vertical amplitudes better than 1 mm at diurnal and semidiurnal frequencies as concluded by [9]. [13] estimated vertical tidal displacements using 3 years of observations derived at 353 globally distributed Global Positioning System (GPS) stations and found a good agreement of GPS observed OTL displacement vertical amplitude and

phase parameters of $M_2$, $N_2$, $S_2$, and $O_1$ constituents with those of model predictions except for $K_1$ and $K_2$ due to multipath effects, solar radiation as well as their high correlation with GPS constellation repeat period and orbital period [16,29,30]. [15] estimated OTL displacement tidal constituents of $M_2$, $S_2$, $N_2$, $O_1$, and $Q_1$ through performing a Kalman filter estimation using 90 days of GPS observations.

In this study, the troposphere delays estimated from 24 hour sessions (external delays) were reduced from the observations a priori to the analysis of 1 hour VLBI sessions of CONT14 campaign. Besides, in the analysis of 1 hour VLBI sessions, the CONT14 specific terrestrial reference frame (TRF) and Earth orientation parameters (EOP) series were used which had been estimated from a global solution through stacking the normal equations of daily sessions of CONT14. By means of handling the estimated hourly station positions as observations along with their formal errors, OTL displacement constituents of principal semi-diurnal and diurnal tides are intended to be resolved.

## 2. IVS CONT14 CAMPAIGN AND ANALYSIS OF HOURLY SESSIONS

International VLBI Service for Geodesy and Astrometry (IVS, [31-33]) carries out 15 days continuous VLBI sessions every three years in order to demonstrate the state-of-art capabilities of the current VLBI technology. Among others, the observations of CONT14 campaign were analyzed for this study, carried out from 6 (0 UT) to 20 (24 UT) May 2014. 17 VLBI stations located at 16 sites were contributed to CONT14 (see Figure 1).

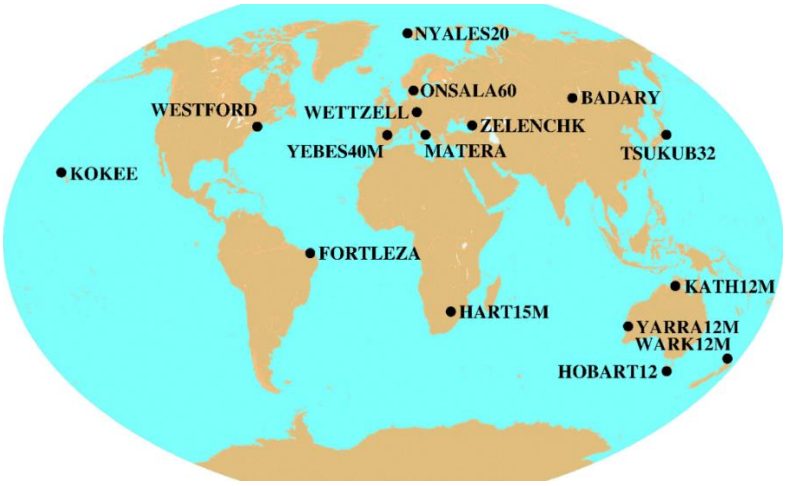


Figure 1. VLBI stations participating to CONT14 campaign [34]

The geodetic VLBI stations contributed to CONT14 campaign are listed in Table 1. For further information on CONT14 campaign readers are referred to [34].

**Table 1:** Geodetic VLBI stations participated to CONT14.

| Observatory name | Country | VLBI Acronym |
|---|---|---|
| Ny-Ålesund | Norway | NYALES20 |
| Onsala | Sweden | ONSALA60 |
| Badary | Russia | BADARY |
| Wettzell | Germany | WETTZELL |
| Zelenchukskaya | Russia | ZELENCHK |
| Westford | USA | WESTFORD |
| Matera | Italy | MATERA |
| Yebes | Spain | YEBES40M |
| Tsukuba | Japan | TSUKUB32 |
| Kokee Park | USA | KOKEE |
| Fortleza | Brazil | FORTLEZA |
| Katherine | Australia | KATH12M |
| Hartebeesthoek | South Africa | HART15M |
| Yarragadee | Australia | YARRA12M |
| Warkworth | New Zealand | WARK12M |
| Hobart | Tasmania | HOBART26 |
| Hobart | Tasmania | HOBART12 |

The high correlation between the parameters in hourly sessions results in troposphere delays and antenna coordinates propagate into each other and unreliable estimates (e.g. [35,36]). To overcome this restriction, external troposphere slant delays $\Delta L$ estimated from 24 hour sessions were reduced from the observations of hourly sessions a priori to the adjustment and residual troposphere delays were not estimated. The CONT14 VLBI observations were analyzed using Vienna VLBI and Satellite Software (VieVS, [37]). The parameters were estimated using classical Gauss Markov least-squares adjustment method. The observations were not removed below a certain elevation angle and not down-weighted. Source coordinates were fixed to ICRF2 (International Celestial Reference Frame, [38]). The high-frequency variations of Earth rotation parameters were modeled as recommended by the IERS Conventions 2010 [39]. Troposphere zenith hydrostatic delays (ZHD) were computed from local surface pressure measurements at the sites using [40-42] and mapped to the observation directions with the VMF1. Tidal and nontidal atmospheric loading [43], as well as tidal ocean loading based on the ocean model FES2014 [2], were introduced to each observation a priori

to the adjustment. Finally, the OTL displacements were assumed to be unveiled by the estimated hourly station positions.

## 3. ESTIMATING THE PRINCIPAL SEMI-DIURNAL AND DIURNAL TIDES FROM THE HOURLY OTL DISPLACEMENTS OBSERVED BY VLBI

The tidal harmonic displacements on the Earth crust, caused by the seafloor pressure variations due to the ocean tide loading (OTL), $\Delta_{n,k}$ for the $k$'th coordinate component (i.e. radial, west, or south) at a site, $n$ and at a particular time $t$ can be formulated with the harmonic function

$$\Delta_{n,k} = \sum_{j} A_{n,j,k} \cos(\chi_j(t) - \varphi_{n,j,k}) \quad (1)$$

where $\chi_j$ denotes the astronomical phase of the $j$'th tidal constituent which is computed from fundamental astronomical arguments [39]. In Eq. 1, $A_{nj}$ and $\varphi_{nj}$ are the amplitude and the phase lag with respect to the $j$'th tidal potential at Greenwich meridian, respectively. Principal lunar semidiurnal tide, $M_2$ is the strongest tidal constituent that has a frequency of 2 cycles per lunar day (period: 12.42 hour). Other principal tides mostly considered are namely; principal solar semidiurnal $S_2$ that has a period of 12 hour, principal lunar elliptic semidiurnal $N_2$ (12.66 hour), lunisolar semidiurnal $K_2$ (11.97 hour that is one-half a sidereal day), lunar diurnal $K_1$ (23.93 hour, one sidereal day), principal solar declination $P_1$ (24.07 hour), principal lunar diurnal $O_1$ (period: 25.82 hour), lunar elliptic diurnal $Q_1$ (26.87 hour), lunisolar fortnightly $M_f$ (13.66 day), lunar monthly evectional constituent $M_m$ (27.55 day), and solar semiannual $S_{sa}$ (182,62 day) [44].

For the calculations of OTL displacements from models according to Eq. 1, the amplitudes and phase lags of principal tides were derived from "Ocean Tide Loading Provider", a web-based facility provided by M.S. Bos and H.-G. Scherneck [45] that uses OLFG/OLMPP algorithm [27] and the Green's functions using Gutenberg-Bullen standard Earth model to determine the deformation due to point loads [46]. Tidal coefficients were selected as not to correct for geocenter motion due to ocean tides. In first place, as a simulation study, hourly OTL displacements were calculated from Eq. 1 using the real and imaginary parts of 342 tidal

constituents that were derived from a spline interpolation of 11 principal tidal constituents as recommended by the IERS2010 conventions [39]. Then, assuming these calculated OTL displacements as observations the amplitudes and phase lags of 8 principal semi-diurnal and diurnal constituents were estimated using the linear form of Eq. 1. Before the estimation, fortnightly, monthly, and semi-annual tidal terms provided from FES2014 were reduced from the hourly positions of the stations. The estimated amplitudes and phase lags of all the 8 semidiurnal and diurnal tides were found as exactly identical to those of the FES2014 model. This one to one agreement suggests that the amplitudes and phases of several semi-diurnal and diurnal principal tidal constituents can be resolved from the 15 days of hourly but errorless OTL displacements even such a short time span of data is highly vulnerable to observational errors. Then, the real hourly series of station positions and their formal errors were used as observations. The results are presented in the following chapter.

## 4. RESULTS AND DISCUSSION

Clear signals of OTL displacements were derived from the hourly station position estimates e.g. the radial component of the geodetic colocation site Kokee is shown in Figure 2. The estimated amplitudes and phases as well as their formal errors of all principal semi-diurnal and diurnal tides at the coastal CONT14 VLBI sites (located in 150 km distance from the coast) are presented in Table 2. Depending on the number and quality of the observations per station, the formal errors of the estimated amplitudes were found similar for most of the tidal constituents, ranging from 0.1 to 0.3 mm in the radial and 0.1 to 0.2 mm in the horizontal components except for the VLBI stations at Hartebeesthoek and Fortaleza of which formal errors of the amplitudes are large about 0.5 mm in radial and 0.3-0.4 mm in horizontal components. The formal errors of the phase angles are found mostly on the order of 5-10 degrees despite for $K_2$, $P_1$ and $Q_1$ tides at the VLBI stations; Hartebeesthoek (HART15M), Fortaleza, Warkworth and Hobart (HOBART12 and HOBART26) they reach up to a few tens of degrees and generally seen in the tangential components. These large formal errors seen on the phases should be resulted from the small amplitudes of these tides.

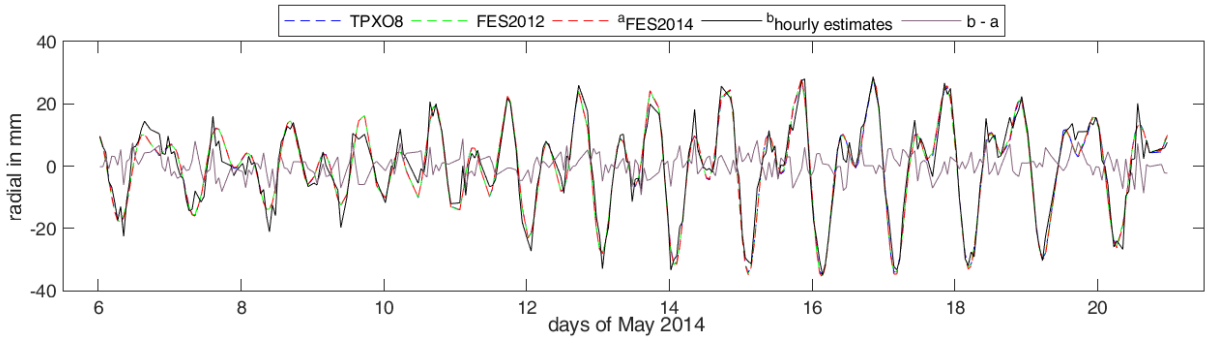


**Figure 2.** *Radial components of the hourly coordinate estimates of KOKEE (Kauai island, Hawaii, USA) station when the ocean tide model corrections were not introduced to the coordinates a priori to the adjustment.*

The best agreement of the estimated radial amplitudes of $M_2$ tide with respect to those of ocean tide models was found at the sites Onsala, Badary, Wettzell, Zelenchukskaya, Matera, Tsukuba, Kokee and Yarragade varying in 0.01-0.40 mm whereas the worst agreement is seen at Fortaleza and Ny-Ålesund and Yebes sites with the radial amplitude differences extend to about 1.5 mm. There are also large discrepancies of $M_2$ tide radial amplitudes between the CONT14 estimates and model values at Hobart and Yebes VLBI sites with the values of about 0.9 mm. At most of the stations, the tangential amplitudes of $M_2$ vary from 0.03 mm (at Matera) to 0.4 mm (at Katherine). It is worth to note that there is a large $M_2$ tide radial amplitude difference of about 0.7 mm between TPXO8 model and both FES2014 and FES2012 models at Ny-Ålesund. When $M_2$ tide Greenwich phase lags are considered, the agreement between estimates and the models do agree within 1 to 5 degrees for most of the stations in all coordinate components. However, the estimated west phases of $M_2$ tide at Badary differ from the models at about 10 degrees as well as at Hartebeesthoek (HART15M) the difference with the model values are on the order of about 13 degrees.

The worst agreement of the estimated radial amplitudes of S2 tide to the model values are seen at the sites Yebes, Hartebeesthoek (HART15M), Fortaleza, and Warkworth ranging in 0.7-2 mm. The agreement of $S_2$ tide at the remaining sites does not exceed 0.4 mm in all components. At all of the sites, the estimated phases of $S_2$ tide are varying in about 5 degrees with respect to those of TPXO8 and FES2014 models whereas at the Ny-Ålesund, Onsala and Wettzell sites the differences in south phases and at Yarragade the difference in radial phase

with respect to FES2012 model are larger with the values of 11.0, 9.2, 10.9, and 7.7 degrees, respectively.

Comparing the level of agreement of the estimated radial amplitudes of $N_2$ tide with respect to the those of ocean tide models 0.2 to 0.3 mm differences are found at most of the sites. Large radial amplitude differences of $N_2$ tide between the estimates and model values at the sites Westford, Fortaleza, and Warkworth are seen as 0.4 mm, 0.5 mm, and 0.8 mm, respectively. Most of the west and south amplitude estimates of $N_2$ tide do not differ from the model predictions more than 0.2 mm. The agreement of estimated $N_2$ phases to those of TPXO8 and FES2014 vary in 5 degrees for all sites, tides and coordinate components while the south components of Westford and Wettzell, and radial component of Badary compared to those of FES2012 are larger about 8, 11 and 10 degrees, respectively.

From the phasor vector plots (see e.g. Figure 3) it can be seen that the agreement of the amplitudes and phases between CONT14 estimates and ocean tide models do agree well for the $M_2$ tide at most of the sites and coordinate components. However, for $K_2$, $P_1$, and $Q_1$ tides at most of the sites and coordinate components CONT14 estimates do not converge to those of the model amplitudes and/or phases. The large formal errors of the estimated amplitudes and phases of $K_2$, $P_1$, and $Q_1$ tidal constituents seen at most the sites also indicate that these tides cannot be well resolved from CONT14 hourly coordinate time series (see also Table 2).

**Table 2:** The amplitudes and phase lags of OTL displacement semi-diurnal and diurnal constituents with their formal errors estimated from CONT14 hourly sessions at coastal stations (located in 150 km distance from the coast) in millimeter and arc degrees, respectively. The stations are sorted from north to south.

| Stations | | $A_{M_2}$ | $\varphi_{M_2}$ | $A_{S_2}$ | $\varphi_{S_2}$ | $A_{N_2}$ | $\varphi_{N_2}$ | $A_{K_2}$ | $\varphi_{K_2}$ | $A_{K_1}$ | $\varphi_{K_1}$ | $A_{O_1}$ | $\varphi_{O_1}$ | $A_{P_1}$ | $\varphi_{P_1}$ | $A_{Q_1}$ | $\varphi_{Q_1}$ |
|---|---|---|---|---|---|---|---|---|---|---|---|---|---|---|---|---|---|
| | R | 9.27±0.11 | 177.3±0.6 | 2.50±0.09 | -141.3±2.1 | 2.05±0.11 | 156.3±2.0 | 0.18±0.09 | -132.9±28.7 | 1.14±0.09 | -46.2±4.6 | 1.40±0.09 | -122.0±3.2 | 0.19±0.11 | 116.6±21.6 | 0.11±0.11 | -161.2±27.7 |
| NYALES20 | W | 2.83±0.06 | -18.2±1.1 | 0.81±0.05 | 34.6±3.8 | 0.60±0.05 | -38.9±4.3 | 0.06±0.05 | 40.9±52.6 | 0.24±0.05 | 103.6±5.6 | 0.47±0.04 | 55.5±5.0 | 0.11±0.06 | 96.3±4.5 | 0.00±0.05 | 163.6±>100 |
| | S | 1.51±0.05 | -23.8±1.9 | 0.58±0.05 | 23.7±4.9 | 0.36±0.05 | -30.9±6.3 | 0.27±0.06 | 25.9±8.1 | 0.83±0.05 | 136.7±3.4 | 0.35±0.05 | 66.3±5.5 | 0.12±0.05 | 127.6±22.1 | 0.06±0.06 | 0.6±9.2 |
| | R | 3.25±0.05 | -64.4±0.8 | 0.87±0.05 | -37.8±3.2 | 0.59±0.06 | -88.0±0.3 | 0.16±0.05 | -39.1±17.2 | 2.11±0.05 | -55.2±1.3 | 1.14±0.06 | -105.5±1.3 | 0.79±0.05 | -56.8±3.1 | 0.09±0.06 | -162.2±18.6 |
| ONSALA60 | W | 1.42±0.05 | 85.1±0.5 | 0.35±0.04 | 118.2±5.7 | 0.19±0.04 | 57.8±9.7 | 0.05±0.04 | 120.7±38.8 | 0.32±0.05 | 96.5±1.9 | 0.43±0.04 | 36.6±5.3 | 0.16±0.05 | 92.0±0.9 | 0.05±0.05 | -0.4±10.9 |
| | S | 0.68±0.05 | 112.7±3.0 | 0.14±0.04 | 142.5±16.5 | 0.18±0.05 | 91.4±0.6 | 0.01±0.04 | 141.8±>100 | 0.26±0.04 | 45.9±9.9 | 0.11±0.05 | -43.7±24.0 | 0.22±0.05 | 37.4±11.6 | 0.06±0.06 | -157.5±31.2 |
| | R | 7.58±0.13 | -168.6±1.0 | 1.51±0.14 | -164.8±4.0 | 1.45±0.16 | 175.4±1.6 | 0.05±0.15 | -165.1±75.0 | 3.43±0.14 | -6.6±2.0 | 2.18±0.14 | 0.8±2.0 | 1.47±0.19 | -4.6±1.7 | 0.34±0.15 | -0.8±2.7 |
| WESTFORD | W | 3.58±0.08 | -129.7±1.3 | 0.31±0.08 | -132.2±13.6 | 0.87±0.08 | -154.2±3.8 | 0.03±0.07 | -139.2±>100 | 0.34±0.09 | -8.1±16.7 | 0.21±0.07 | 24.3±16.9 | 0.05±0.14 | -2.0±33.8 | 0.16±0.06 | 43.0±22.7 |
| | S | 1.84±0.10 | -18.0±2.8 | 0.52±0.10 | 18.1±8.1 | 0.50±0.09 | -31.4±8.1 | 0.12±0.10 | -158.3±28.3 | 0.25±0.10 | 176.5±18.8 | 0.16±0.08 | -48.2±24.0 | 0.18±0.14 | -176.6±9.3 | 0.03±0.10 | 10.6±60.9 |
| | R | 7.79±0.10 | 50.3±0.7 | 3.84±0.10 | 70.3±0.8 | 1.13±0.10 | 64.1±3.4 | 0.74±0.10 | 66.7±4.5 | 9.65±0.09 | -137.2±0.6 | 7.34±0.09 | -154.0±0.6 | 4.39±0.10 | -139.9±1.3 | 0.72±0.11 | -166.0±3.2 |
| TSUKUB32 | W | 2.59±0.08 | -10.7±1.8 | 1.24±0.08 | 30.1±3.5 | 0.43±0.08 | -22.8±6.9 | 0.41±0.09 | 25.9±8.1 | 2.02±0.09 | -169.4±2.4 | 1.51±0.08 | 172.8±2.0 | 1.08±0.12 | -172.0±2.0 | 0.13±0.08 | 160.4±17.1 |
| | S | 1.92±0.05 | -76.7±0.8 | 0.58±0.05 | -63.9±3.7 | 0.46±0.06 | -84.6±1.0 | 0.09±0.05 | -66.1±20.4 | 1.43±0.06 | 90.7±0.1 | 1.20±0.05 | 70.4±1.4 | 1.01±0.06 | 87.9±0.2 | 0.08±0.04 | 52.6±30.5 |
| | R | 12.19±0.23 | -121.2±1.0 | 4.42±0.25 | -118.9±2.4 | 2.10±0.21 | -127.6±5.4 | 0.98±0.22 | -128.3±12.4 | 10.60±0.24 | 60.9±1.1 | 6.04±0.20 | 54.9±1.8 | 4.91±0.23 | 59.6±2.1 | 0.72±0.20 | 50.2±15.5 |
| KOKEE | W | 2.92±0.19 | 153.8±3.6 | 0.81±0.20 | -172.3±10.7 | 0.52±0.18 | 156.0±13.5 | 0.01±0.24 | -171.7±>100 | 2.05±0.17 | 38.7±4.7 | 1.30±0.18 | 12.7±5.4 | 0.93±0.18 | 36.4±10.6 | 0.08±0.20 | 0.3±19.6 |
| | S | 4.41±0.14 | 97.3±0.5 | 1.55±0.12 | 126.4±4.1 | 0.71±0.15 | 93.0±0.9 | 0.30±0.13 | 119.0±18.8 | 1.68±0.13 | 111.9±2.7 | 1.23±0.14 | 93.5±0.6 | 0.75±0.14 | 108.1±5.1 | 0.10±0.15 | 82.5±16.2 |
| | R | 36.85±0.41 | 33.5±0.6 | 9.48±0.39 | 55.4±2.1 | 8.14±0.46 | 20.9±1.8 | 2.22±0.37 | 52.2±9.0 | 1.88±0.50 | 96.9±2.7 | 2.46±0.39 | 32.3±7.8 | 1.86±0.47 | 90.4±0.1 | 0.36±0.51 | 174.9±11.4 |
| FORTLEZA | W | 5.14±0.34 | 22.3±3.1 | 1.52±0.28 | 43.9±10.7 | 0.49±0.40 | 8.0±11.0 | 0.83±0.29 | 39.7±19.0 | 0.14±0.32 | 155.2±>100 | 0.34±0.35 | -14.4±28.7 | 0.44±0.28 | 139.1±36.4 | 0.02±0.28 | 138.8±>100 |
| | S | 5.80±0.30 | 51.4±2.8 | 1.67±0.36 | 83.6±2.1 | 1.24±0.31 | 27.7±10.4 | 0.65±0.34 | 82.4±5.7 | 0.75±0.29 | 123.6±19.8 | 0.94±0.34 | 95.4±2.9 | 0.29±0.28 | 119.2±43.2 | 0.33±0.32 | 73.2±24.0 |
| | R | 3.56±0.16 | 146.7±2.3 | 0.42±0.15 | -110.6±11.4 | 0.81±0.17 | 104.4±4.5 | 0.29±0.15 | -115.5±19.3 | 7.61±0.18 | 11.7±0.9 | 6.06±0.16 | 8.9±0.8 | 3.57±0.19 | 10.3±1.0 | 0.83±0.17 | -0.3±1.1 |
| YARRA12M | W | 2.27±0.12 | -128.5±2.8 | 0.75±0.12 | -72.4±4.5 | 0.58±0.12 | -152.9±8.6 | 0.20±0.13 | -72.8±16.2 | 1.53±0.12 | 148.4±4.2 | 0.56±0.10 | 144.3 ±10.0 | 0.82±0.12 | 145.9±7.4 | 0.05±0.10 | 136.6±>100 |
| | S | 2.52±0.14 | -158.7±3.2 | 0.84±0.15 | -99.4±2.6 | 0.49±0.17 | -179.5±4.4 | 0.10±0.15 | -104.5±33.2 | 0.64±0.13 | -66.3±7.8 | 0.45±0.14 | -103.5±6.6 | 0.17±0.16 | -73.8±22.4 | 0.06±0.12 | -118.3±88.8 |
| | R | 26.15±0.19 | 56.7±0.4 | 4.42±0.19 | 121.2±2.1 | 3.71±0.19 | 30.0±2.3 | 0.64±0.19 | 116.1±11.4 | 3.72±0.22 | -174.0±1.9 | 0.56±0.21 | 118.6±16.1 | 2.10±0.27 | -179.0±1.1 | 0.08±0.19 | 47.9±>100 |
| WARK12M | W | 8.58±0.15 | -21.5±0.9 | 0.94±0.19 | 8.1±7.5 | 1.89±0.12 | -40.9±3.6 | 0.31±0.20 | -12.6±13.4 | 0.60±0.14 | -23.6±12.9 | 0.76±0.12 | -62.5±7.2 | 0.27±0.16 | -28.1±25.5 | 0.17±0.15 | -86.2±5.0 |
| | S | 5.73±0.19 | 18.5±1.7 | 1.02±0.17 | 31.3±8.7 | 1.38±0.23 | -0.9±1.6 | 0.09±0.20 | -155.5±85.6 | 0.90±0.17 | -148.2±9.5 | 0.56±0.20 | -174.2±8.9 | 0.66±0.20 | -153.6±12.0 | 0.10±0.20 | 172.7±22.5 |
| | R | 10.34±0.16 | 151.7±0.8 | 0.97±0.16 | -114.2±5.9 | 2.62±0.14 | 130.3±2.9 | 0.03±0.15 | 56.4±>100 | 6.54±0.17 | 86.5±0.1 | 5.64±0.13 | 56.5±1.2 | 2.99±0.16 | 79.6±0.8 | 1.02±0.12 | 44.7±6.9 |
| HOBART26 | W | 4.26±0.12 | 103.5±0.7 | 1.86±0.10 | 135.0±3.2 | 0.61±0.12 | 105.8±4.6 | 0.65±0.10 | 129.7±8.7 | 0.94±0.13 | -161.1±5.7 | 0.37±0.12 | -161.4±11.7 | 0.62±0.14 | -162.9±6.3 | 0.11 ±0.13 | -175.3±10.1 |
| | S | 1.11±0.15 | 103.6±3.3 | 0.40±0.15 | 98.2±4.7 | 0.07±0.16 | 92.6±8.7 | 0.12±0.18 | -84.2±12.2 | 1.12±0.13 | -142.6±6.4 | 1.15±0.15 | -162.8±4.4 | 0.71±0.14 | -145.4±10.1 | 0.30±0.17 | -174.0±5.3 |
| | R | 10.14±0.16 | 152.0±0.8 | 1.05±0.15 | -114.1±5.3 | 2.50±0.13 | 130.4±3.0 | 0.04±0.15 | -123.0±>100 | 6.33±0.17 | 86.5±0.1 | 5.83±0.13 | 56.4±1.1 | 2.85±0.17 | 79.5±0.9 | 1.08±0.12 | 44.6±6.5 |
| HOBART12 | W | 4.35±0.14 | 103.2±0.8 | 1.64±0.12 | 134.9±4.1 | 0.64±0.13 | 105.8±4.9 | 0.39±0.11 | 129.8±16.1 | 0.99±0.15 | -160.2±6.3 | 0.18±0.13 | -161.7±27.2 | 0.37±0.16 | -163.0±11.7 | 0.03±0.15 | 8.1±58.3 |
| | S | 1.05±0.16 | 103.7±3.7 | 0.38±0.16 | 98.2±5.4 | 0.08±0.17 | 92.6±8.1 | 0.33±0.18 | -84.2±4.5 | 1.18±0.14 | -142.7±6.5 | 1.31±0.16 | -164.6±4.0 | 1.13±0.14 | -145.4±6.5 | 0.41±0.17 | -174.2±4.0 |

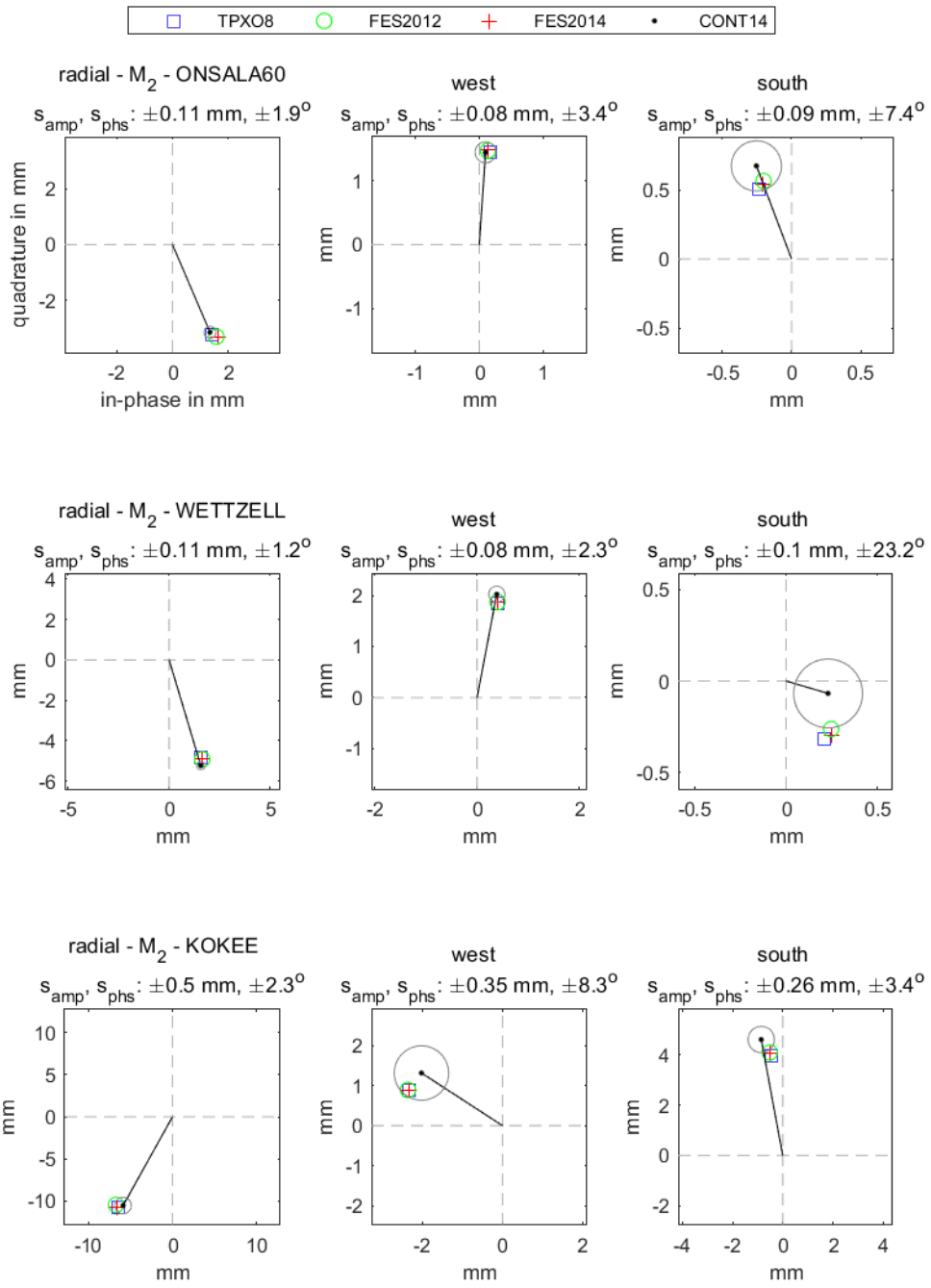


***Figure 3.*** *Phasor vectors of OTL displacement $M_2$ constituent with one sigma error ellipses at ONSALA60 (Sweden), WETTZELL (Germany) and KOKEE (Hawaii, USA) stations. The horizontal axis represents the in-phase component, and the vertical axis the out-of-phase component relative to the tidal potential at Greenwich. The Greenwich phase lag is zero along the positive direction in the horizontal axis and the phase angle increases counterclockwise.*

## 5. CONCLUSION

The amplitudes of phasor vector differences between CONT14 estimates and those of ocean tide models are below 0.4 mm at the inland sites: Badary, Wettzell, Matera and Zelencuhkskaya as well as at the coastal site Onsala for all principal semi-diurnal and diurnal tides. The worst agreement between CONT14 estimates and ocean tide models in terms of phasor vector differences are seen at the sites Warkworth and Fortaleza where the differences in radial components for both semi-diurnal and diurnal tides vary in 0.8 to 2.0 mm. The latter is due to the high humidity during the CONT14 period that results in the errors of troposphere delays to propagate to the estimated OTL displacements. While the large median formal errors of the hourly coordinate estimates at station Warkworth as 8.1 mm, 4.8 mm, and 7.5 mm in radial, south, and west directions might results in the radial amplitudes of the phasor vector differences to vary in 0.5-1.5 mm at all tides.

As an overall assessment, the RMS of the radial amplitudes of phasor vector differences (radial RMS misfits) between the CONT14 estimates and those of ocean tide models i.e. FES2014, FES2012 and TPXO8 is found about two times larger than those of tangential components. Likewise, the RMS misfits over coastal stations are about two times larger than those of inland stations for all tides. The best agreement between CONT14 and considered ocean tide models in radial component is seen for $N_2$ tide with the RMS misfits of about 0.2 mm across inland sites and 0.4 mm across the coastal sites. The amplitudes and phases between CONT14 and ocean tide models do partly agree for $S_2$, $N_2$, $K_1$, and $O_1$ tides at most of the sites and coordinate components. However, for $K_2$, $P_1$, and $Q_1$ tides CONT14 estimates mostly do not converge to those of the model amplitudes and/or phases.

Unmodeled portions of troposphere delays comprise the largest part of the total errors in the observations of space geodetic techniques and significantly propagate to the station coordinates when station coordinates are estimated at sub-diurnal intervals. To improve the accuracies of semi-diurnal and diurnal tidal constituents, estimated from a short time span of sub-daily station coordinates, further developments on the troposphere delay model is necessary.

## ACKNOWLEDGEMENT

This work is supported by The Scientific and Technological Research Council of Turkey (TÜBİTAK), project number: 115Y244. The author acknowledges the International VLBI Service for Geodesy and Astrometry for providing the observations of CONT14 campaign.

## REFERENCES

**1.** Agnew, D.C. SPOTL: Some Programs for Ocean-Tide Loading, SIO Technical Report 2012, Scripps Inst of Oceanogr., University of California.

**2.** Carrère, L.; Lyard, F.; Cancet, M.; Guillot, A.; Picot, N. Finite Element Solution FES2014, a new tidal model - Validation results and perspectives for improvements, presentation to ESA Living Planet Conference, 2016, Prague.

**3.** Lyard, F.; Lefevre, F.; Letellier, T.; Francis, O. Modelling the global ocean tides: Modern insights from FES2004. Ocean Dyn 2006, 56(5-6), 394-415.

**4** Carrère, L.; Lyard, F.; Cancet, M.; Guillot, A.; Roblou, L. A new global tidal model taking advantage of nearly 20 years of altimetry. In: Proceedings of Meeting "20 Years of Altimetry", 2012, Venice.

**5.** Egbert, G.D.; Erofeeva, S.Y. Efficient inverse modeling of barotropic ocean tides. Journal of Atmospheric and Oceanic Technology 2002, 183-204.

**6.** Egbert, G.D.; Erofeeva, S.Y.; Ray, R.D. Assimilation of altimetry data for nonlinear shallow-water tides: Quarter-diurnal tides of the Northwest European Shelf. Cont Shelf Res 2010, 30(6), 668-679.

**7.** Foreman, M. Manual for tidal heights analysis and prediction. Pac Mar Sci Rep 1977, 77–10, 1–58.

**8.** Schuh, H.; Möhlmann, L. Ocean loading station displacements observed by VLBI. Geophys Res Lett 1989, 16:1105-1108.

**9.** Sovers, O.J. Vertical ocean loading amplitudes from VLBI measurements. Geophys Res Lett 1994, 21, 357-360.

**10.** Haas, R.; Schuh, H. Ocean loading observed by geodetic VLBI. In Proceedings of the 13th International Symposium on Earth Tides 1998, edited by B. Ducarme and P. Paquet, pp 111-120.

**11.** Scherneck, H.G.; Haas, R.; Laudati, A. Ocean loading for, in and from VLBI. In IVS 2000 General Meeting Proceedings 2000, Greenbelt, edited by N. Vandenberg and K. Baver, 257-262.

**12.** Dach, R.; Dietrich, R. The Ocean Loading Effect in the GPS Analysis: A Case Study in the Antarctic Peninsula Region. Marine Geodesy 2001, 24:1, 13-25.

**13** Schenewerk, M.S.; Marshall, J.; Dillinger, W. Vertical ocean-loading deformations derived from a global GPS network. J Geod Soc Jpn 2001, 47(1), 237–242.

**14.** Petrov, L.; Ma, C.P. Study of harmonic site position variations determined by very long baseline interferometry. J Geophys Res 2003, 108(B4):2190.

**15.** Allinson, C.R.; Clarke, P.J.; Edwards, S.J.; King, M.A.; Baker, T.F.; Cruddace, P.R. Stability of direct GPS estimates of ocean tide loading. Geophys Res Lett 2004, 31, L15603.

**16.** King, M.A.; Penna, N.T.; Clarke, P.J.; King, E.C. Validation of ocean tide models around Antarctica using onshore GPS and gravity data. J Geophys Res 2005, 110, B08401.

**17.** Thomas, I.D.; King, M.A.; Clarke, P.J. A comparison of GPS, VLBI and model estimates of ocean tide loading displacements. J Geod 2007, 81(5), 359-368.

**18.** Yuan, L.; Chao, B.F.; Ding, X.; Zhong, P. The tidal displacement field at Earth's surface determined using global GPS observations. J Geophys Res Solid Earth 2013, 118, 2618-2632.

**19.** Vey, S.; Calais, E.; Llubes, M.; Florsch, N.; Woppelmann, G.; Hinderer, J.; Amalvict, M.; Lalancette, M.F.; Simon, B.; Duquenne, F.; Haase, J.S. GPS measurements of ocean loading and its impact on zenith tropospheric delay estimates: a case study in Brittany, France. J Geod 2002, 76, 419-427.

**20.** Khan, S.A.; Scherneck, H.G. The M2 ocean tide loading wave in Alaska: Vertical and horizontal displacements, modelled and observed. J Geod 2003, 77(3– 4), 117–127.

**21.** King, M.A. Kinematic and static GPS techniques for estimating tidal displacements with application to Antarctica. J Geodyn 2006, 41(1-3), 77-86.

**22.** Yun, H.S.; Lee, D.H.; Song, D.S. Determination of vertical displacements over the coastal area of Korea due to the ocean tide loading using GPS observations. J Geodyn 2007, 43(3-5), 528-541.

**23.** Melachroinos, S.A.; Biancale, R.; Llubes, M.; Perosanz, F.; Lyard, F.; Vergnolle, M.; Bouin, M.N.; Masson, F.; Nicolas, J.; Morel, L.; Durand, S. Ocean tide loading (OTL) displacements from global and local grids: comparisons to GPS estimates over the shelf Brittany, France. J Geod 2008, 82(6), 357-371.

**24.** Vergnolle, M.; Bouin, M.N.; Morel, L.; Masson, F.; Durand, S.; Nicolas, J.; Melachroinos, S.A. GPS estimates of ocean tide loading in NW-France: Determination of

ocean tide loading constituents and comparison with a recent ocean tide model. Geophys J Int 2008, 173(2), 444-458.

**25.** Penna, N.T.; Clarke, P.J.; Bos, M.S.; Baker, T.F. Ocean tide loading displacements in western Europe: 1. Validation of Kinematic GPS estimates. J Geophys Res Solid Earth 2015, 120, 6523-6539.

**26.** Martens, H.R.; Simons, M.; Owen, S.; Rivera, L. Observations of ocean tidal response in South America from subdaily GPS positions. Geophys J Int 2016, 205, 1637-1664.

**27.** Scherneck, H.G. A parameterized solid earth tide model and ocean tide loading effects for global geodetic baseline measurements. Geophys J Int 1991, 106(3):677-694.

**28.** Pagiatakis, S.D. The response of a realistic earth to ocean tide loading. Geophys J Int 1990, 103, 541-320.

**29.** Urschl, C.; Dach, R.; Hugentobler, U.; Schaer, S.; Beutler, G. Validating ocean tide loading models using GPS. J Geod 2005, 78(10):616-625.

**30.** Zhong, P.; Ding, X.L.; Yuan, L.G.; Xu, Y.L.; Kwok, K.; Chen, Y.Q. Sidereal filtering based on single differences for mitigating GPS multipath effects on short baselines. J Geod 2010, 84: 145-158.

**31.** Nothnagel, A.; Artz, T.; Behrend, D.; Malkin Z. International VLBI Service for Geodesy and Astrometry - Delivering high-quality products and embarking on observations of the next generation. J Geod 2019, 91(7), 711–721.

**32.** Behrend, D. Data Handling within the International VLBI Service. Data Science Journal 2013, Vol. 12, pp. WDS81–WDS84.

**33.** Schuh, H.; Behrend, D. VLBI: A fascinating technique for geodesy and astrometry. J Geodyn 2012, 61, 68–80.

**34.** International VLBI Service for Geodesy and Astrometry. Available online: https://ivscc.gsfc.nasa.gov/index.html (accessed on 4 August 2019).

**35.** Rothacher, M.; Beutler, G. The Role of GPS in the study of Global Change. Physics and Chemistry of the Earth 1998, 23(9/10):1029-1040.

**36.** Teke, K.; Böhm, J.; Nilsson, T.; Krasna, H. Sub-daily antenna position estimates from the CONT11 campaign. Proceedings of the 21st Meeting of the European VLBI Group for Geodesy and Astrometry (EVGA), Reports of the Finnish Geodetic Institute 2013, edited by N. Zubko and M. Poutanen, Helsinki, Finland, 131-134.

**37.** Böhm, J.; Böhm, S.; Boisits, J.; Girdiuk, A.; Gruber, J.; Hellerschmied, A.; Krasna, H.; Landskron, D.; Madzak, M.; Mayer, D.; McCallum, J.; McCallum, L.; Schartner, M.; Teke, K. Vienna VLBI and Satellite Software (VieVS) for Geodesy and Astrometry. Publications of the Astronomical Society of the Pacific 2018, 130(986), 044503; 1 – 6.

**38.** Fey, A.; Gordon, D.; Jacobs, C.S. The second realization of the International Celestial Reference Frame by Very Long Baseline Interferometry. IERS Technical Note 2009, vol. 35. Verlag des BundesamtsfürKartographie und Geodasie, Frankfurt am Main, ISBN 3-89888-918-6.

**39.** Petit, G.; Luzum, B. IERS Conventions 2010, IERS Technical Note 2010; 36. Verlag des Bundesamts für Kartographie und Geodasie, Frankfurt am Main.

**40.** Saastamoinen, J. Atmospheric correction for the troposphere and stratosphere in radio ranging of satellites. In the use of artificial satellites for geodesy, Geophys Monogr Ser 1972, 15, Amer. Geophys. Union, 274–251.

**41.** Saastamoinen, J. Contribution to the theory of atmospheric refraction (in three parts). Bull Geod 1973, 105–107, 279–298.

**42.** Davis, J.L.; Herring, T.A.; Shapiro, I.I.; Rogers, A.E.E.; Elgered, G. Geodesy by radio interferometry: effects of atmospheric modeling errors on estimates of baseline length. Radio Sci 1985, 20 (6), 1593–1607.

**43.** Petrov, L.; Boy, J.P. Study of the atmospheric pressure loading signal in Very Long Baseline Interferometry observations. J Geophys Res 2004, 109 (B3), B03405.

**44.** Doodson, A.T. The Harmonic Development of the Tide-Generating Potential. Proceedings of the Royal Society A: Mathematical, Physical and Engineering Sciences 1921, 100 (704): 305-329.

**45.** Ocean tide loading provider – Chalmers. Available online: http://holt.oso.chalmers.se/loading (accessed on 4 August 2019).

**46.** Farrell, W.E. Deformation of the Earth by surface loads. Rev Geophys Space Phys 1972, 10(3):761-797.